Validation of Coupled Eddy Current-Thermal Simulations for Induction Infrared Thermographic Non-Destructive Testing

M. Bakry*, R.A. Biezemans*,**, E. Demaldent*, O. Ghibaudo*, A. Vigneron*

** Université Paris Saclay, CEA, List, F-91120, Palaiseau, France*
*** Corresponding author*

Abstract

Over the course of the last years, induction thermography has been identified as a promising method for non-destructive testing (NDT) and a possible alternative to manual and pollutant techniques such as dye penetrant or magnetic particle inspection. To study the effect of the many parameters that influence an induction thermography NDT set up, the CEA-List institute is developing a computational model for the full simulation chain of eddy current generation, heat diffusion and infrared camera response. This contribution focuses on the coupling of the eddy current and thermal simulation and presents a first comparison between the computational model and measured data.

1. Computational model

Recent work illustrates the importance of numerical modelling for the design of NDT procedures [1]. Indeed, computer simulations avoid the costly and time-consuming task of producing specimens with artificial defects and allow finer control over, e.g., the defect dimensions, than is possible with manufactured defects. Building on its long-standing experience in eddy current computations within the CIVA simulation platform [2], dedicated to the simulation of inspection techniques by a variety of excitation sources, the CEA-List institute is currently developing a 3D model for the complete induction thermography measurement chain: eddy current generation, thermal diffusion and thermal radiation towards the infrared camera. The goal is to give access to key quantities of interest in CIVA, such as the measured temperature evolution over time and the phase contrast, while keeping the overall simulation time limited.

The eddy current model relies on a boundary element method [3] and allows to compute the generated heating power at the surface of the specimen. The volumetric heating can be computed in a post-processing step, but this is computationally expensive. The results of such a power computation are illustrated in **Figure 1**. The thermal solver, on the other hand, is a volumetric model based on the highly efficient Alternating Direction Implicit method [4]. This requires the heat to be computed in the volume. The chosen coupling strategy consists of a highly-resolved volume computation of the generated Joule heating in the proximity of the defect and a simplified model based on a plane-wave approximation of the electromagnetic field in the sound area, where the field varies smoothly.

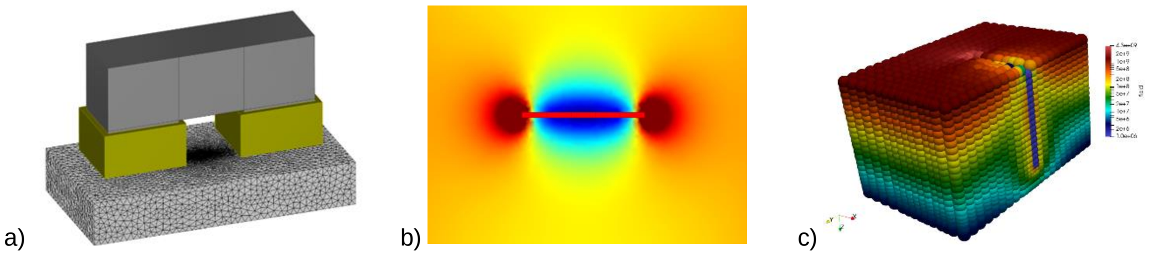

Figure 1. Induction power computation. a) Prototypical configuration consisting of a U-shaped yoke placed around a slot. b) Computed surface power density around a notch defect. c) Computed power density in the volume around the defect.

2. Comparison with experimental results

A first comparison between the induction thermography simulation and experimental data is currently in progress. The chosen set up consists of an Inconel plate of thickness 1.55 mm with a manufactured through slot of length 10 mm and width 0.1 mm. The depth of the artificial notch defects is variable (1.55, 1.24, 0.93, 0.62, and 0.31 mm). Induction heating is applied with a U-ferritic yoke surmounted by a copper winding consisting of 36 turns. A weight is placed on top of the yoke to mitigate vibration effects. The infrared radiation flux is measured with the long-wavelength uncooled infrared camera EDECAM at an observation angle of 45° to avoid reflections from the environment. The full set up is shown in Figure 2. A first comparison is made between the numerically computed temperature and the camera response of the experimental set up. In accordance with the Stefan-Boltzmann law, the fourth root of the camera output is considered. Other effects that influence camera response (such as the viewing angle and surface emissivity) are not accounted for in the simulation results considered here.

a) b) c)
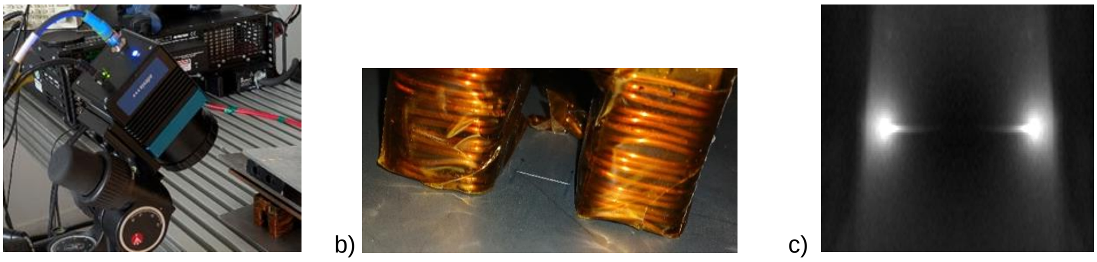

Figure 2. Experimental set up. a) Infrared thermography bench, specimen, inductor and infrared camera. b) Zoom on the inductor and a manufactured defect. c) Example of an acquired infrared image during heating.

Figure 3a shows the measured and simulated data for the temperature offset on a line segment between the yoke legs 0.4 mm below the defect, 25 ms after a heating pulse of 100 ms at an induction frequency of 20 kHz was applied. Both the measured and simulated curves are normalized so that the maximum signal on the inspected line at the end of the heating pulse equals 1. Along with the data along the inspected line, the variation of the data within 0.15 mm is also shown to take into account possibly imperfect spatial alignment, noise and pixelization of the experimental data. **Figure 3b** compares the measured and simulated data in a point at a distance of 0.6 mm below the defect tip over time for different durations of the heating pulse. For the experimental data, the variation over the surrounding pixels is also included in the figure. All signals are normalized with respect to the maximum value for the longest heating time, since the measured data then contains the smallest relative noise level.

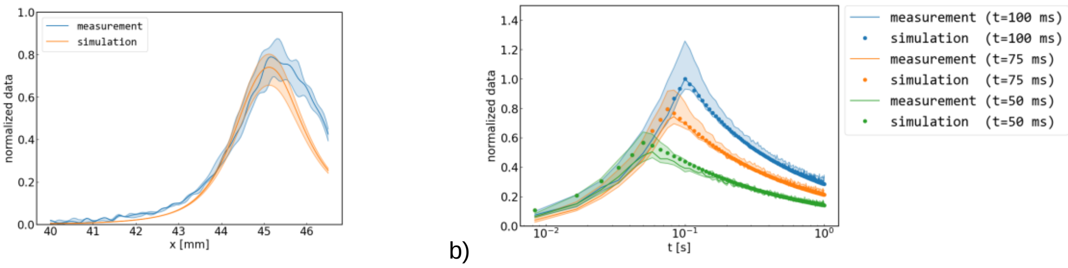

a) b)

Figure 3. Comparison of experimental and simulated temperature offset after an induction heating pulse. a) Temperature offset along a line between the yoke legs below the defect at 25 ms after a pulse of 100 ms. b) Time evolution of the temperature at 0.6 mm below the defect tip for different pulse durations.

3. Conclusion and discussion

Satisfactory agreement for a first comparison between experimental and simulated data has been observed. However, the extent of agreement varies over the specimen's surface, and future work will focus on identifying possible explanations for this, such as the influence of electric and thermal properties of the material and geometric and experimental parameters. The computational model will further be corroborated by a comparison with established simulation software and experimental comparison with different heat sources.

References

[1] B. Oswald-Tranta, 'Detection and characterisation of short fatigue cracks by inductive thermography', *Quant. InfraRed Thermogr. J.*, vol. 19, no. 4, pp. 239–260, 2022, doi: 10.1080/17686733.2021.1953226.

[2] EXTENDE, 'CIVA, NDT Simulation Software', CIVA, NDT Simulation Software. Accessed: Jun. 08, 2026. [Online]. Available: https://www.extende.com/civa-ndt-simulation-software/

[3] M. Bonnet and E. Demaldent, 'Eddy-current asymptotics of the Maxwell PMCHWT formulation for multiple bodies and conductivity levels', *Comput. Math. Appl.*, vol. 141, pp. 80–101, 2023, doi: 10.1016/j.camwa.2023.03.026.

[4] J. Douglas, 'Alternating direction methods for three space variables', *Numer. Math.*, vol. 4, no. 1, pp. 41–63, 1962, doi: 10.1007/BF01386295.

Acknowledgements

This work was supported by ANR PIA funding: ANR-20-IDEES-0002.